Precise Dispensing of Liquids Using Visual Feedback

Monroe Kennedy III, Kendall Queen, Dinesh Thakur, Kostas Daniilidis, and Vijay Kumar

Abstract— Robotic pouring is an important step in improving the safety, productivity and repeatability in the biotechnology industry and generally increasing the effectiveness of robotics in human based environments. In this work we present a method to autonomously dispense a precise amount of fluid using only visual feedback without using precision pouring instruments such as pipettes, syringes or pourers. We model circular and rectangular pouring container geometries. We prove that for square containers we can control the flow by only observing the fluid height in the receiving beaker. We show a systematic approach using a hybrid control scheme that is robust to the initial amount of fluid in the pouring container and inconsistent flow. Specifically we present (a) a model for pouring (b) a model based algorithm to drive a robot arm (c) visual feedback for regulating the pouring rate. We demonstrate this using the Rethink Robotics Sawyer manipulator and mvBluefox MLC202bc camera.

I. INTRODUCTION

One of the main goals in robotics is to assist in repetitive, laborious, and dangerous tasks. Precise pouring of fluids can easily fall under each of these categories, examples being manipulation of hazardous biological fluids, molten metal in the casting industry, or even the assembly of buffers and solvents in wet lab research. In each of these examples a common requirement is that a specified amount of fluid be poured with precision to a desired amount.

To achieve these precise motions required for pouring, researchers have used learning models to perform reinforcement and imitation learning to pour [1], [2], [3]. While effective, limitations of these methods are the number of trials required to learn the pouring task, reliance on empirical results rather than on analytical guarantees of system performance, and inability to generalize learned model.

One approach to perform smooth pouring is to minimize sloshing of the liquid while pouring a predetermined trajectory. Some research proves to suppress sloshing while pouring using a hybrid shape approach which consists of proportional gain, notch and a low pass filter [4], [5], [6], [7]. In this approach, the control input consists of feed forward expression based on the proposed model, and the hybrid shape to mitigate sloshing during the pour [6], [7], [8]. Noda and Terashima tried to overcome the requirement for the need of an analytical inverse of the dynamical function by using a numerical look up table for the desired height [9] and corresponding input. In the above model based examples [8], [9] load cells were used to provide real time feedback on poured fluid mass.

GRASP Lab, University of Pennsylvania, Pennsylvania, PA 19104
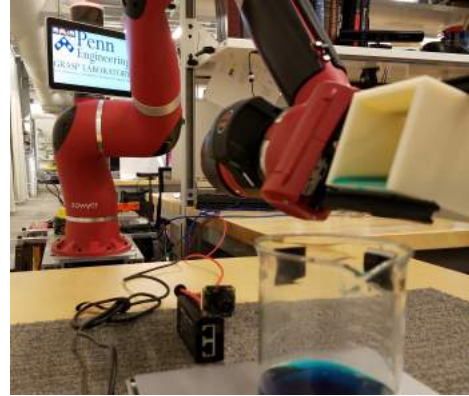Email: (kmonroe, queen, tdinesh, kostas, kumar)@seas.upenn.edu

Fig. 1: Experimental setup using the Rethink Robotics Sawyer manipulator to pour precise amounts of water into a beaker using vision for feedback control.

Vision is also used for real time feedback by detecting how much fluid is currently in the pouring container, or in transit. Mottaghi et al. present a method using learning to estimate the volume of containers and the amount of fluid inside them using vision [10]. Yamaguchi et al. present a method using stereo vision and optical flow to track fluids being poured during flight between containers [11]. The most recent approach in [12] is the state of the art in liquid perception because it tracks the liquid while it is poured as well as the amount in the container using a recurrent neural network. Compared to our approach [12] is superior in the perception but more simplistic in the control and without providing any analytical proof.

Our proposed method extends previous work in that it is analytically based and we provide a closed form expression for the control input using a hybrid controller and feedback linearization. We also show that we are able to detect the height of the fluid using vision, and due to our pouring container design specifications, we only need to observe along with the angle of the pouring container, the height or mass of the fluid in the receiving container and its derivative. By using a minimum jerk trajectory for the fluid height, we are able to ensure smooth motion for our end-effector and fluid height [13]. The rest of the paper is organized as follows, Section II-A describes the general pouring model. Section II-B presents our specific system design and justification. Section II-C describes our method of visual feedback to detect the fluid height. Section III shows our results and discussion for implementing this method on the Rethink Robotics Sawyer manipulator shown in Figure 1.
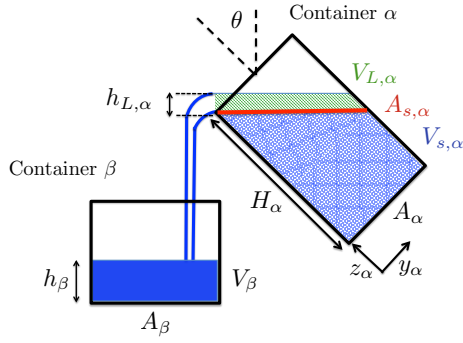
Fig. 2: The Pouring Problem: For a fluid poured from container α to container β with specified geometric parameters, the goal is to pour a precise amount of fluid using visual or weight feedback based on an analytical model and closed form control.

II. METHODOLOGY

A. General Pouring Model

We propose a simple model to characterize smooth flow between two open containers. We assume as in [7] that the fall time of the fluid between the containers is negligible. Consider a pouring container α and receiving container β, with respective volumes V_α, V_β respectively as shown in Figure 2. For container β, the height of fluid h_β and cross sectional area $A_\beta(z_\beta)$ parameterized by the height in the body fixed frame coordinate, together they define the volume

$$V_\beta = \int_0^{h_\beta} A_\beta(z_\beta) dz_\beta. \tag{1}$$

For the pouring container α, the maximum volume of the container is defined as $V_\alpha = \int_0^{H_\alpha} A_\alpha(z_\alpha)$ as shown in Figure 2, where H_α is the height of the container, and $A_\alpha(z_\alpha)$ is the cross sectional area parameterized by the body frame coordinate. When container α is rotated by angle θ, there will be a volume of the fluid above the pouring lip $V_{L,\alpha}$, and volume below the pouring lip $V_{s,\alpha}$, separated by a surface area $A_{s,\alpha}(\theta)$ as shown in Figure 2. The height of the fluid above the lip is defined as $h_{L,\alpha}$, and, for small heights, the volume is approximated as in [8], [9] by

$$V_{L,\alpha} \simeq h_{L,\alpha} A_{s,\alpha}(\theta). \tag{2}$$

The volume below the surface can be found by integrating the cross sectional area from the base of the container to the dividing surface $A_{s,\alpha}$, which defines the volume $V_{s,\alpha}$

$$V_{s,\alpha} = \int A_\alpha(z_\alpha) dz_\alpha. \tag{3}$$

The dividing surface $A_{s,\alpha}$ is a function of the angle θ, container geometry and volume of fluid below the surface $V_{s,\alpha}$. Assuming the only degree of freedom is θ, then θ, its derivative $\omega = \dot\theta$ or higher order derivatives must be controlled to produce the desired flow rate and poured volume.

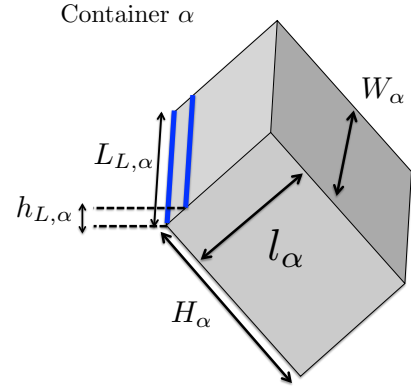Fig. 3: Pouring geometry used to derive analytical model.

The flow rate between the two containers α and β is defined as $q[\frac{m^3}{s}]$. In relation to the respective volumes, the flow rate is defined by

$$q = \dot V_\beta = -\dot V_\alpha = -(\dot V_{L,\alpha} + \dot V_{s,\alpha}). \tag{4}$$

By expanding this differentiation based on transient terms for container α, the flow rate (4) becomes (5). Note that the partial derivatives of $A_{s,\alpha}, V_{s,\alpha}$ are required as they are not explicitly a function of time

$$\begin{aligned} q &= -\dot h_{L,\alpha} A_{s,\alpha} - h_{L,\alpha} \frac{\partial A_{s,\alpha}}{\partial \theta}\omega - \frac{\partial V_{s,\alpha}}{\partial \theta}\omega \\ &= \left(A_\beta(h_\beta) + h_\beta \frac{\partial A_\beta(h_\beta)}{\partial h_\beta}\right)\dot h_\beta. \end{aligned} \tag{5}$$

To express $h_{L,\alpha}$, we define the area of the pouring mouth as $A_L = h_{L,\alpha} L_{L,\alpha}(h_{L,\alpha})$, where $L_{L,\alpha}(h_{L,\alpha})$ is the line of the opening of the mouth at varying heights (as shown in Figure 3 where in this case it is a constant). We note that the height $h_{L,\alpha}$ is related to the flowrate by Bernoulli's principle $\frac{v^2}{2} + gz + \frac{P}{\rho} = const.$ where v, z, P, ρ are the fluid velocity, height, pressure and density respectively at a particular point in the steady, streamline flow. We consider Bernoulli's principle acting on volume $V_{L,\alpha}$. The fluid at the top surface of this volume has no velocity, whereas the volume at the bottom (height $h_{L,\alpha}$ below the surface) has a velocity $V = \sqrt{2gh_{L,\alpha}}$. As flow rate is defined as $q[\frac{m^3}{s}]$ or $[m^2 \cdot \frac{m}{s}]$, we can integrate over the pouring area to obtain the flowrate

$$q = A_L(h)v(h) = \int_0^{h_{L,\alpha}} L_{L,\alpha}(h)\sqrt{2gh}\,dh. \tag{6}$$

By differentiating this with respect to time, we can obtain an expression for $\dot h_{L,\alpha}$ in terms of flow rate $q, \dot q$. Given these fundamental equations, we consider different container designs to ensure effective state observation, system model simplicity and ultimately control.

B. Specific Pouring Model Using Rectangular Container Geometry

Design considerations for the pouring container α include the pouring lip and container geometry. The terms that are

Fig. 4: We use the Rethink Robotics Sawyer manipulator to precisely pour colored water into a beaker using visual feedback from a mvBluefox MLC202bc camera.

directly related to these factors are the lip length $L_{L,\alpha}(h_{L,\alpha})$, flow rate $q(h_{L,\alpha})$, dividing area $A_{s,\alpha}(\theta)$, and volume below the lip $V_{s,\alpha}(\theta)$.

Considering three cases: a rectangular lip where the length is constant, v-shaped lip that has an opening angle γ, and circular lip shape, where the entire opening has a radius R, the lip shape equations become

$$L_{L,\alpha,rect}(h) = L_{L,alpha} \tag{7}$$

$$L_{L,\alpha,vshape}(h) = 2h\cos(\frac{\gamma}{2}) \tag{8}$$

$$L_{L,\alpha,circ}(h) = 2\sqrt{h(2R-h)}. \tag{9}$$

The flow rate q for circular and rectangular lip geometries are shown in (10), (11) and are found by integrating (6)

$$q_{rect} = \frac{2}{3}L_{L,\alpha}\sqrt{2g}h_{L,\alpha}^{\frac{3}{2}} \tag{10}$$

$$q_{circ} = -\frac{4\sqrt{2g}}{15}\left(128R^5 - 120R^3h_{L,\alpha}^2 \right.$$
$$\left. +20R^2h_{L,\alpha}^3 + 30Rh_{L,\alpha}^4 - 9h_{L,\alpha}^5\right). \tag{11}$$

Differentiating these flow rates with respect to time produces

$$\dot{q}_{rect} = L_{L,\alpha}\sqrt{2g}h_{L,\alpha}^{\frac{1}{2}}\dot{h}_{L,\alpha} \tag{12}$$

$$\dot{q}_{circ} = \frac{-4\sqrt{2g}}{15}\left(\left(-240R^3h_{L,\alpha} + 60R^2h_{L,\alpha}^2 \right.\right.$$
$$\left.\left. +120Rh_{L,\alpha}^3 - 45h_{L,\alpha}^4\right)\right)\dot{h}. \tag{13}$$

Note that by substituting $h_{L,\alpha}$ from (10) into (12) we can express (12) as

$$\dot{h}_{L,\alpha} = \left(\frac{2}{3}\right)^{\frac{1}{3}}L^{-\frac{2}{3}}(2g)^{-\frac{1}{3}}q^{-\frac{1}{3}}\dot{q}. \tag{14}$$

For the dividing area $A_{s,\alpha}$, we consider two cases: a square and circular container. In both instances the cross sectional area is constant in body frame z_α. The dividing area $A_{s,\alpha}$ is defined to consist of a major and minor axis a, b, where rotation occurs about the minor axis b. In the case of a circular container the area of an ellipse is πab, Hence the respective areas are shown in (15), (16), where a' is the elongated axis as a function of the angle θ

$$A_{s,\alpha,circ} = \pi a'b = \pi ab\sec(\theta) \tag{15}$$

$$A_{s,\alpha,rect} = a'b = ab\sec(\theta), \tag{16}$$
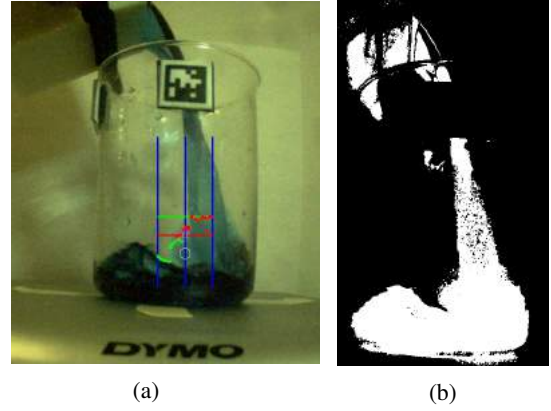

(a)   (b)

Fig. 5: Robustness of our vision method to sloshing in fast trajectories, tracking and foreground images. The height is estimated as minimum of purple and white rings (K-means cluster centers), in Figure 5a estimated height is the white ring.

differentiation with respect to time produces

$$\dot{A}_{s,\alpha,circ} = \pi ab\tan(\theta)\sec(\theta)\omega \tag{17}$$

$$\dot{A}_{s,\alpha,rect} = ab\tan(\theta)\sec(\theta)\omega. \tag{18}$$

The volume of fluid below the dividing surface $V_{s,\alpha}$ is shown in (19) for rectangular geometry. Note that while other geometries can be found, this volume is straight forward. Using the geometry notation shown in Figure 3, with container width W_α, length l_α, total height H_α

$$V_{s,\alpha,rect} = \int_0^{l_\alpha}\int_0^{H(y)}\int_0^{W_\alpha}dxdzdy$$
$$= \int_0^{l_1}W_\alpha H(y)dy = \int_0^{l_1}W_\alpha(H_b - y\tan(\theta))dy$$
$$= W_\alpha H_\alpha l_\alpha - \frac{l_\alpha^2}{2}W_\alpha\tan(\theta). \tag{19}$$

The derivative with respect to time produces

$$\dot{V}_{s,\alpha,rect} = -\frac{l_\alpha^2 W_\alpha}{2}\sec^2(\theta)\omega. \tag{20}$$

Given these parameterizations, we will now show that the design configuration in Figure 3 allows for a concise representation of the dynamical system in (5) in Proposition (1).

Proposition 1: By using an open, rectangular pouring container α as shown in Figure 3, and container β with constant cross sectional area A_β, we can represent (5) in terms of only transient variables $h_\beta, \dot{h}_\beta, \theta, \omega$.

Proof: Using equations (7), (10), (12), (14), (16), (18),

(20) assuming constant A_β, (5) becomes

$$q = -\left(\left(\frac{2}{3}\right)^{\frac{1}{3}} L_{L,\alpha}^{-\frac{2}{3}} (2g)^{-\frac{1}{3}} q^{-\frac{1}{3}} \dot{q}\right) (W_\alpha l_\alpha \sec(\theta))$$
$$- \left(\left(\frac{3}{2}\right)^{\frac{2}{3}} L_{L,\alpha}^{-\frac{2}{3}} (2g)^{-\frac{1}{3}} q^{\frac{2}{3}}\right) (W_\alpha l_\alpha tan(\theta) \sec(\theta)\omega)$$
$$+ \frac{l_\alpha^2 W_\alpha}{2} \sec^2(\theta)\omega. \tag{21}$$

Solving for $\dot{q}$ produces Equation (22)

$$\dot{q} = -3^{\frac{1}{3}} L_{L,\alpha}^{\frac{2}{3}} g^{\frac{1}{3}} W_\alpha l_\alpha \sec(\theta) q^{\frac{4}{3}}$$
$$- \frac{3}{2} \tan(\theta) q\omega$$
$$+ \left(\frac{3}{8}\right)^{\frac{1}{3}} l_\alpha \sec(\theta) L_{L,\alpha}^{\frac{2}{3}} g^{\frac{1}{3}} q^{\frac{1}{3}} \omega, \tag{22}$$

using the relation in (23) we obtain the relation between $\dot{q}$ and $\ddot{h}_\beta$

$$\dot{q} = A_\beta \ddot{h}_\beta. \tag{23}$$

Substituting Equation (23) and $q = A_\beta \dot{h}_\beta$ into Equation (21) produces Equation (24) whose transient terms are only $h_\beta, \dot{h}_\beta, \theta, \omega$.

$$\ddot{h}_\beta = -3^{\frac{1}{3}} L_{L,\alpha}^{\frac{2}{3}} g^{\frac{1}{3}} W_\alpha l_\alpha \sec(\theta) A_\beta^{\frac{1}{3}} \dot{h}_\beta^{\frac{4}{3}}$$
$$- \frac{3}{2} \tan(\theta) \dot{h}_\beta \omega$$
$$+ \left(\frac{3}{8}\right)^{\frac{1}{3}} l_\alpha \sec(\theta) L_{L,\alpha}^{\frac{2}{3}} g^{\frac{1}{3}} A_\beta^{\frac{-2}{3}} \dot{h}_\beta^{\frac{1}{3}} \omega \tag{24}$$

We define $Q_1(\theta), Q_2(\theta), Q_3(\theta)$

$$Q_1(\theta) = -3^{\frac{1}{3}} L_{L,\alpha}^{\frac{2}{3}} g^{\frac{1}{3}} W_\alpha l_\alpha \sec(\theta) \tag{25}$$

$$Q_2(\theta) = -\frac{3}{2} \tan(\theta) \tag{26}$$

$$Q_3(\theta) = \left(\frac{3}{8}\right)^{\frac{1}{3}} l_\alpha sec(\theta) L_{L,\alpha}^{\frac{2}{3}} g^{\frac{1}{3}}, \tag{27}$$
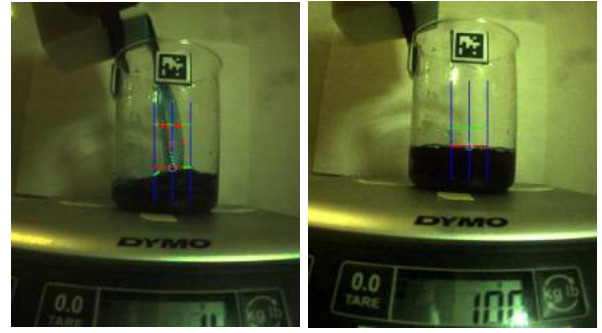
which simplifies (24) to

$$\ddot{h}_\beta = Q_1(\theta) A_\beta^{\frac{1}{3}} \dot{h}_\beta^{\frac{4}{3}} + \left(Q_2(\theta)\dot{h}_\beta + Q_3(\theta)A_\beta^{-\frac{2}{3}} \dot{h}_\beta^{\frac{1}{3}}\right) \omega. \tag{28}$$

■

With these design parameters we have derived a component of the system dynamics, we now define the region on which it is controllable and the hybrid controller used.

Theorem 1: For a experimental setup defined in Proposition 1, with system states $\begin{bmatrix} x_1 & x_2 & x_3 \end{bmatrix}^T = \begin{bmatrix} h_\beta & \dot{h}_\beta & \theta \end{bmatrix}^T$ and input $u = \omega$, there exists a hybrid control input that allows for control of the system in the domain $\mathcal{D} : x_3 \in (-\frac{\pi}{2}, \frac{\pi}{2})$ for states $\vec{x}_0$ starting in $\mathcal{D}$.

Proof: The full system dynamics based on (28) is

$$\begin{bmatrix} \dot{x}_1 \\ \dot{x}_2 \\ \dot{x}_3 \end{bmatrix} = \begin{bmatrix} |x_2| \\ Q_1(x_3)A^{\frac{1}{3}}x_2^{\frac{4}{3}} \\ 0 \end{bmatrix} + \begin{bmatrix} 0 \\ Q_2(x_3)x_2 + Q_3(x_3)A^{-\frac{2}{3}}x_2^{\frac{1}{3}} \\ 1 \end{bmatrix} u, \tag{29}$$

(a) (b)

Fig. 6: Using background subtraction, Sobel gradient detection and K-means clustering (Figure 6a) we are able to track the top of the fluid for feedback control. In Figure 6b the goal was to pour 100ml.

which takes the general form $\dot{x} = f(x) + g(x)u$. To determine the region on which this is feedback linearizable we must determine the conditions of full rank for the matrix M defined in (30), where $ad_f g(x)$ represents the adjoint $[f, g]$ (lie bracket). And is also feedback linearizable if the span M's vectors are involutive

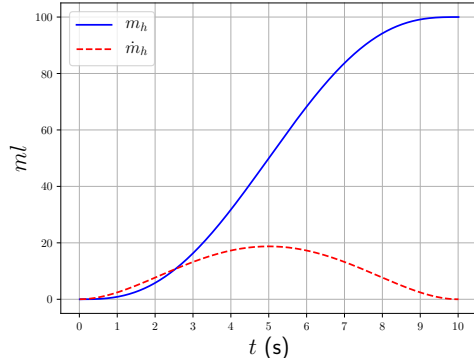$$M = \begin{bmatrix} g(x) & ad_f g(x) & ad_f^2 g(x) \end{bmatrix}. \tag{30}$$

The matrix M has full rank when $x_2 \neq 0$, meaning the height must be changing. Also we can see by inspection that $g(x)$ is only left invertible when $x_3 \neq -\frac{\pi}{2}$ or $x_3 \neq \frac{\pi}{2}$. Hence we propose the following hybrid controller

$$u = \begin{cases} g(x)^\dagger(\tau - f(x)) & x_2 \neq 0 \text{ and } x_3 \in (-\frac{\pi}{2}, \frac{\pi}{2}) \\ sgn(x_3)\delta_\omega & x_2 = 0 \text{ and } x_3 \in (-\frac{\pi}{2}, \frac{\pi}{2}) \\ 0 & x_3 \notin (-\frac{\pi}{2}, \frac{\pi}{2}), \end{cases} \tag{31}$$
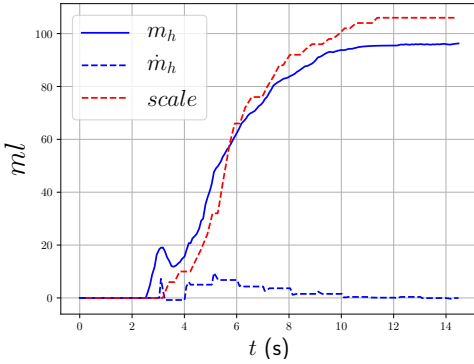
where the domain conditions here serve as hybrid control guard and reset function constraints, and these functions are an identity map. Using feedback linearization the system reduces to a second order ordinary differential equation, and solving for the desired state x_1 will exponentially approach the desired point also in D for positive proportional and derivative gains K_p, K_d. We define the term τ to be this input, and have it consist of a feedback and feed forward term prescribed by the desired trajectory of $x_1(t)$

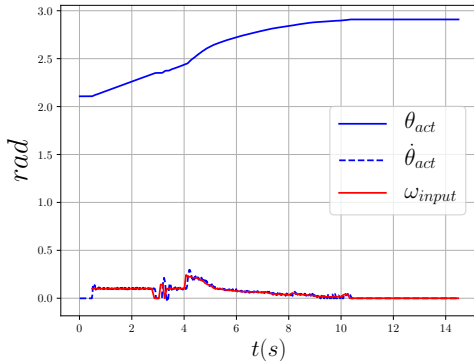$$\tau = \ddot{x}_{1,des} + K_p(x_{1,des} - x_1) + K_d(\dot{x}_{1,des} - \dot{x}_1). \tag{32}$$

The desired trajectory for the system is a minimum jerk trajectory for the state x_1 which defines $\ddot{x}_{1,des}, \dot{x}_{1,des}, x_{1,des}$ where $\ddot{x}_{1,des}$ is the feed forward term. We define a smooth, sigmoid trajectory for the fluid height by using a 5th order polynomial. Such a polynomial with specified end points characterizes a minimum jerk trajectory, and inherently minimizes the change in accelerations while respecting the boundary constraints. The specified endpoints are the initial height and final height both with zero velocity and acceleration. These boundary constraints fully define the trajectory in closed form [13]. Therefore with (31), (32) we can track the specified trajectory in domain D.

■

(a)

(b)

(c)

Fig. 7: We verify our model using an ODE solver in Figure 7a, we then perform this same trajectory on the real system shown in Figures 7b, 7c.

It is noted in [14] that motions that minimize jerk are also effective in suppressing vibrations in a mechanical transfer system. Hence, a minimum jerk trajectory is an adequate candidate to achieve smooth pouring, which is a necessary consideration for the steady flow assumption of the Bernoulli equation. However, it is important to note that our method does not require that the flow remain steady, as we use a hybrid controller to handle instances when flow is interrupted. But the minimum jerk trajectory produces long periods of steady flow as shown in experiments. It must also be noted that a minimum jerk trajectory alone does not ensure there will be no sloshing, and in the event of very aggressive pours it would be advantageous to compensate.
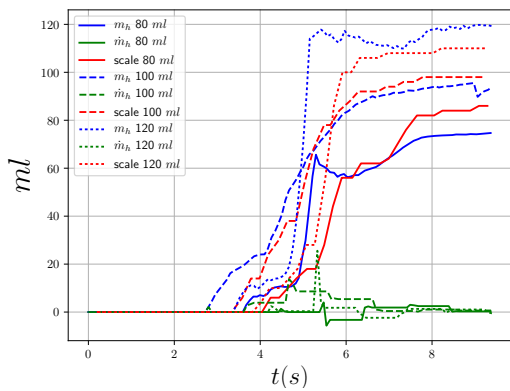
In practice, the dynamics of the fluid (and sloshing) can be modeled using the Navier-Stokes equations, but the motion of the fluid as a whole in the container can be approximated with a analogous (spherical) pendulum model [15], [16]. The limitation of existing methods is that it is assumed the natural frequency (which is dependent on the current volume and container shape) of the fluid remains constant, but in a pouring scenario the frequency fluctuates when the volume of liquid changes. In the cases where the fluid volume remains constant, input shapers as shown in [15] or the hybrid shape approach (utilizing notch filters for matching the fluid natural frequencies with the notch resonance frequencies) as shown in [6], can be used to minimize sloshing during quick motions. So in the case of aggressive pouring, an input shaper, particularly zero vibration (ZD) shaper which uses two impulse inputs with delay between them which is a function of the natural frequency and dampening ratio (volume specific) can be used to mitigate sloshing. A study of these input shapers and their convolutions to minimize sloshing is studied in depth for a square container in [17] and hence may be useful in very aggressive trajectories where either the natural frequency modes can be approximated as constant, or updated based on container pose and current volume, with the initial applied angular accelerations (or jerks) used to model an impulse input. In this work, we examine pours whose sloshing is sufficiently suppressed by the choice of minimum jerk trajectories.
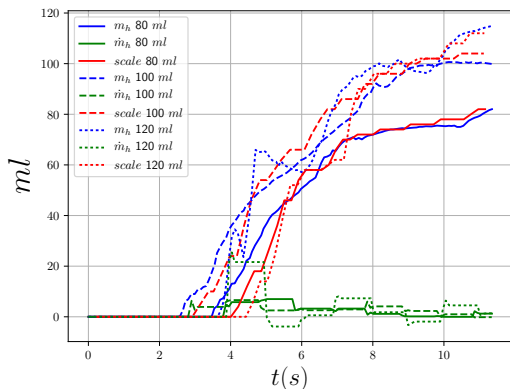
C. Visual Feedback

We perform visual feedback on the height of the fluid in the receiving beaker by tracking the top of the fluid. Using a fiducial, we locate the beaker in the field of view. After locating, we then utilize the OpenCV background subtracter which is a Gaussian mixture-based background/foreground segmentation algorithm [18]. Once the foreground is obtained, we then use a Sobel operator to find the gradient in the image. We then perform K-means clustering on the given gradient to segment the pixels under the tag into at most two clusters a) those for falling water b) those for rising water as shown in Figure 5 and 6. By using the cluster which is always lowest we increase the probability of tracking the top of the fluid, even in extreme cases of rigorous sloshing which occurs in fast pours, for example Figure 5.
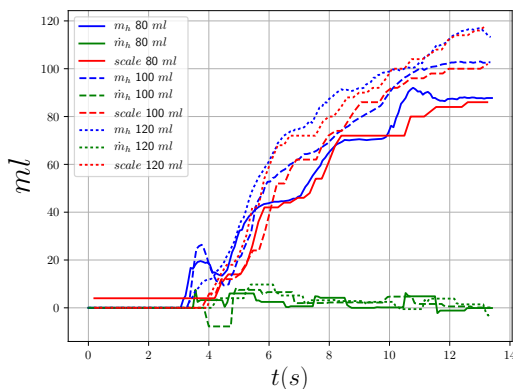
III. RESULTS AND DISCUSSION

In our experimental setup shown in Figure 4, we used the Rethink Robotics Sawyer manipulator to pour dyed water into a beaker. We performed visual feedback using a mvBluefox MLC202bc camera and verified the reported volume with a DYMO Digital Postal Scale M25. We used Apriltag fiducials developed by Ed Olson to locate the beaker in the image frame [19]. The Sawyer robot runs at 100Hz, we ran the camera at 12Hz, the scale runs at 5Hz. While

(a) 8 second trajectory

(b) 10 second trajectory

(c) 12 second trajectory

Fig. 8: Representative experimental trials of pouring. The trials are for pouring 80, 100, and 120ml, over three different time intervals.

the camera rate could be increased, we did not observe significant improvement in performance.

We demonstrate our detection method is robust to sloshing which occurs during fast trajectories as shown in Figure 5. The detection method is also robust to instances when the incoming fluid crosses the region of interest Figure 6a. To achieve these, we track the fluid directly under the tag, and only from the current estimate of the height to a threshold distance above that point. This threshold distance moves with the estimated height (shown as the green line in Figures 5a,
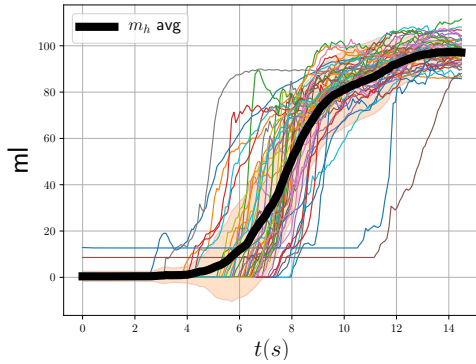
6a, 6b). The red line in these images indicates the goal height. We show the estimated height at the indicated desired height in Figure 6b.

While our vision height estimates are in cm, given the area of the beaker we convert this to an expected volume in ml. In the following plots, we will reference this mass height as m_h and it is the computed ml volume from a given height, which allows us to represent the expected height and scale ground truth in same units. We verify our model using an ode solver shown in Figure 7a, then perform this same trajectory on the actual system shown in Figures 7b, 7c. In Figure 8, we pour 80, 100, 120ml each with 8, 10, 12s trajectories. It can be noted that with longer trajectories and larger volumes the accuracy increases. In Figure 9a, we present 50 trials of 100ml pours with 10s trajectories. Contributions to variance include the fact that the pouring container did not always contain the same initial amount of fluid, hence the hybrid controller provides a constant positive velocity until pouring begins, then the trajectory is initialized at the onset of pouring.
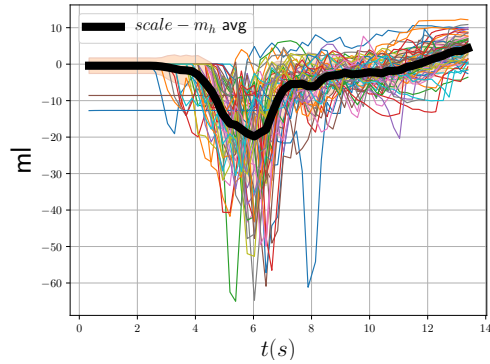
This demonstrates the robustness of our hybrid control to the amount of fluid in the pouring container. It can also be seen that there are points where the pouring height levels off. This is due to the fact that during some pours, there were bubbles forming on the side of the glass, which causes the vision algorithm to report a higher than actual height. When this occurred, the system would halt until either the bubbles popped and it continued, or until the trajectory indicated a higher height was required than that estimated. In either event the system recovers and pours the desired amount with the reported variance. Figure 9b shows the error between the visual volume estimation and the reported scale. It can be noted that across all 50 trials there is a consistent peak in the difference at the beginning of the pours. We attribute this to the fact that because we keep the camera at a constant height, when the fluid level is observed from above the surface of the fluid can offset the reported height, but as the level of the fluid approaches the height of the camera, the reported value increases in accuracy. While backing the camera away from the setup would reduce this disparity, it would also serve to reduce resolution. A video demonstrating this method and the results can be found on Youtube: "Precise Dispensing of Liquids Using Visual Feedback (GRASP Lab UPenn)".

IV. CONCLUSIONS

In this work, we present a hybrid controller capable of precision pouring using visual feedback. Our fluid height detection algorithm performs online background subtraction to obtain the foreground, then tracking the region of the image under the Apriltag we perform K-means clustering with two clusters to distinguish between fluid entering the beaker and the rising height of the fluid. We show that our detection algorithm is robust to sloshing in the receiving beaker. Our controller is robust to the initial amount of fluid in the pouring container. Our controller is also robust to halts in fluid flow which occur due to errors in estimation caused by sloshing or bubbles. In these instances the controller relies

(a) 10 second trajectory　　　　　　　(b) 10 second trajectory

Fig. 9: Figure 9a 50 Trials pouring 100ml for 10s trajectories. Black line is average, shaded region is 1st standard deviation. Figure 9b average and standard deviation between scale and vision report of height. Consistent dip is due to detection of the top of the fluid at the beginning of the pour from camera perspective registering as higher heights.

on its hybrid nature to re-initiate flow to pour the precise amount. Future work includes developing an adaptive hybrid controller capable of being agnostic to container geometries given the general flowrate (5). Another extension would be to consider using a moving camera for tracking the height of the fluid to ensure the camera is always level with the detected fluid height, which is a technique used by humans to pour exact amounts.

ACKNOWLEDGMENT

REFERENCES

[1] M. Tamosiunaite, B. Nemec, A. Ude, and F. Wörgötter, "Learning to pour with a robot arm combining goal and shape learning for dynamic movement primitives," *Robotics and Autonomous Systems*, vol. 59, no. 11, pp. 910–922, 2011.

[2] L. Kunze, A. Haidu, and M. Beetz, "Acquiring task models for imitation learning through games with a purpose," in *Intelligent Robots and Systems (IROS), 2013 IEEE/RSJ International Conference on*. IEEE, 2013, pp. 102–107.

[3] L. Rozo, P. Jiménez, and C. Torras, "Force-based robot learning of pouring skills using parametric hidden markov models," in *Robot Motion and Control (RoMoCo), 2013 9th Workshop on*. IEEE, 2013, pp. 227–232.

[4] K. Yano, T. Toda, and K. Terashima, "Sloshing suppression control of automatic pouring robot by hybrid shape approach," in *Decision and Control, 2001. Proceedings of the 40th IEEE Conference on*, vol. 2. IEEE, 2001, pp. 1328–1333.

[5] M. Kaneko, Y. Sugimoto, K. Yano, and K. Terashima, "Supervisory control of pouring process by tilting-type automatic pouring robot," in *Intelligent Robots and Systems, 2003.(IROS 2003). Proceedings. 2003 IEEE/RSJ International Conference on*, vol. 3. IEEE, 2003, pp. 3004–3009.

[6] Y. Noda, K. Yano, and K. Terashima, "Control of self-transfer-type automatic pouring robot with cylindrical ladle," *IFAC Proceedings Volumes*, vol. 38, no. 1, pp. 295–300, 2005.

[7] Y. Sugimoto, K. Yano, and K. Terashima, "Liquid level control of automatic pouring robot by two-degrees-of-freedom control," *IFAC Proceedings Volumes*, vol. 35, no. 1, pp. 137–142, 2002.

[8] T. Tsuji and Y. Noda, "High-precision pouring control using online model parameters identification in automatic pouring robot with cylindrical ladle," in *Systems, Man and Cybernetics (SMC), 2014 IEEE International Conference on*. IEEE, 2014, pp. 2563–2568.

[9] Y. Noda and K. Terashima, "Falling position control of outflow liquid for automatic pouring system with tilting-type ladle," *IFAC Proceedings Volumes*, vol. 40, no. 11, pp. 53–58, 2007.

[10] R. Mottaghi, C. Schenck, D. Fox, and A. Farhadi, "See the glass half full: Reasoning about liquid containers, their volume and content," *arXiv preprint arXiv:1701.02718*, 2017.

[11] A. Yamaguchi and C. G. Atkeson, "Stereo vision of liquid and particle flow for robot pouring," in *Humanoid Robots (Humanoids), 2016 IEEE-RAS 16th International Conference on*. IEEE, 2016, pp. 1173–1180.

[12] C. Schenck and D. Fox, "Visual closed-loop control for pouring liquids," *CoRR*, vol. abs/1610.02610, 2016. [Online]. Available: http://arxiv.org/abs/1610.02610

[13] M. Zefran, V. Kumar, and C. B. Croke, "On the generation of smooth three-dimensional rigid body motions," *IEEE Transactions on Robotics and Automation*, vol. 14, no. 4, pp. 576–589, 1998.

[14] K. Hoshijima and M. Ikedo, "Vibration suppression control for mechanical transfer systems by jerk reduction," *INTERNATIONAL JOURNAL OF CONTROL AUTOMATION AND SYSTEMS*, vol. 5, no. 6, p. 614, 2007.

[15] W. Aribowo, T. Yamashita, and K. Terashima, "Integrated trajectory planning and sloshing suppression for three-dimensional motion of liquid container transfer robot arm," *Journal of Robotics*, vol. 2015, p. 3, 2015.

[16] A. AlSaibie and W. Singhose, "Experimental testing of liquid slosh suppression in a suspended container with compound-pendulum dynamics," in *Control Conference (ASCC), 2013 9th Asian*. IEEE, 2013, pp. 1–6.

[17] Q. Zang and J. Huang, "Dynamics and control of three-dimensional slosh in a moving rectangular liquid container undergoing planar excitations," *IEEE Transactions on Industrial Electronics*, vol. 62, no. 4, pp. 2309–2318, 2015.

[18] Z. Zivkovic, "Improved adaptive gaussian mixture model for background subtraction," in *Proceedings of the Pattern Recognition, 17th International Conference on (ICPR'04) Volume 2 - Volume 02*, ser. ICPR '04. Washington, DC, USA: IEEE Computer Society, 2004, pp. 28–31. [Online]. Available: http://dx.doi.org/10.1109/ICPR.2004.479

[19] E. Olson, "AprilTag: A robust and flexible visual fiducial system," in *Proceedings of the IEEE International Conference on Robotics and Automation (ICRA)*. IEEE, May 2011, pp. 3400–3407.